

The Arabidopsis *STICHEL* Gene Is a Regulator of Trichome Branch Number and Encodes a Novel Protein¹

Hilmar Ilgenfritz², Daniel Bouyer², Arp Schnittger, Jaideep Mathur, Victor Kirik, Birgit Schwab, Nam-Hai Chua, Gerd Jürgens, and Martin Hülskamp*

Zentrum für Molekularbiologie Pflanzen, Entwicklungs-genetik, Universität Tübingen, Auf der Morgenstelle 1, D-72076 Tübingen, Germany (H.I., D.B., A.S., B.S., G.J., M.H.); University of Köln, Botanical Institute III, Gyrhofstrasse 15, 50931 Köln, Germany (J.M., V.K., M.H.); and Rockefeller University, 1230 York Avenue, New York, New York 10021 (N.-H.C.)

Here, we analyze the *STICHEL* (*STI*) gene, which plays an important role in the regulation of branch number of the unicellular trichomes in Arabidopsis. We have isolated the *STI* locus by positional cloning and confirmed the identity by sequencing seven independent *sti* alleles. The *STI* gene encodes a protein of 1,218 amino acid residues containing a domain with sequence similarity to the ATP-binding eubacterial DNA-polymerase III γ -subunits. Because endoreduplication was found to be normal in *sti* mutants the molecular function of *STI* in cell morphogenesis is not linked to DNA replication and, therefore, postulated to represent a novel pathway. Northern-blot analysis shows that *STI* is expressed in all organs suggesting that *STI* function is not trichome specific. The analysis of *sti* alleles and transgenic lines overexpressing *STI* suggests that *STI* regulates branching in a dosage-dependent manner.

Formally, cell shape can be considered to be established in three steps (Hülskamp et al., 1998). In a first step, spatial information, e.g. cell polarity, is established by intracellular mechanisms or provided by outer cues. In a second step, this information is used to reorganize the cell, e.g. change the cytoskeletal arrangement. Finally, actual growth takes place, which includes the incorporation of membrane and cell wall material at defined areas of the cell periphery.

Although some of the biochemistry of the last two steps of the cytoskeletal function and cell wall synthesis is known, the mechanisms underlying the spatial control of cell morphogenesis are largely elusive. Single-cell model systems such as pollen tubes, root hairs, and leaf hairs (trichomes) that are accessible to genetic approaches provide the means to study spatial control mechanisms (Aeschbacher et al., 1994; Marks, 1997; Oppenheimer, 1998; Hülskamp et al., 1999; Kost et al., 1999; Wilhelmi and Preuss, 1999). Among these model cell types, trichomes in Arabidopsis are particularly well suited because they consistently develop a complex three-dimensional form, thus providing excellent criteria to isolate mutants affecting discrete aspects of morphogenesis (Oppenheimer, 1998; Hülskamp et al., 1999).

Leaf trichomes in Arabidopsis are large single cells that originate from the epidermis and are up to 500 μm tall. After trichome fate commitment the cells stop dividing but continue DNA synthesis (endoreduplication; Hülskamp et al., 1994). The incipient trichome extends out of the leaf surface and undergoes two successive branching events (Hülskamp et al., 1994). The orientation of the first branching is co-aligned with the proximal-distal leaf axis. The primary branch, which points toward the leaf tip (main stem), undergoes a second branching in a plane perpendicular to the primary branching plane (Folkers et al., 1997). Subsequently, the trichome extensively elongates concomitant with an increase in vacuolization. The mature trichome has, on average, a DNA content of 32 C, suggesting that trichomes proceed through four endoreduplication cycles (Hülskamp et al., 1994).

Trichome branching requires the coordinated action of at least 18 genes (Marks, 1997; Oppenheimer, 1998; Hülskamp et al., 1999). One group of genes appears to affect primarily the number of endoreduplication cycles and probably, as a consequence, also branch number (Hülskamp et al., 1994; Perazza et al., 1999; Kirik et al., 2001). A second group of branching mutants affects branch number without affecting endoreduplication (Folkers et al., 1997; Luo and Oppenheimer, 1999; Qiu et al., 2002). The genetic analysis of branching mutants suggests that branch formation is controlled by several redundant pathways (Luo and Oppenheimer, 1999).

To date, five branching genes have been cloned and all appear to be involved in the regulation of the microtubule cytoskeleton at different levels. The *ZWI* (*ZWICHEL*) gene encodes a kinesin motor protein

¹ This work was supported by a Leibnitz award (to G.J.), by the Volkswagen Stiftung (grant to M.H.), and by an Schwerpunktprogram Cell Polarity grant (to M.H.).

² These authors contributed equally to the paper.

* Corresponding author; e-mail martin.huelskamp@uni-koeln.de; 49-0221-470-5062.

Article, publication date, and citation information can be found at www.plantphysiol.org/cgi/doi/10.1104/pp.014209.

with a calmodulin-binding domain, indicating that microtubule-based transport is important for branch formation (Oppenheimer et al., 1997). That the spatial organization of microtubules is important for trichome branching is suggested by the finding that in *an* (*angustifolia*) mutants, reduced trichome branching is correlated with the failure to establish a higher microtubule density at the tip of the developing trichome (Folkers et al., 2002). The underlying biochemical mechanism, however, remains unclear because AN encodes a novel protein with sequence similarity to C-terminal binding protein/BrefeldinA ribosylated substrates that are known to be involved in transcriptional regulation or in vesicle budding but not in microtubule function (Folkers et al., 2002; Kim et al., 2002). The *FRA2* (*FRAGILE FIBER2*)/*ERH3* (*ECTOPIC ROOT HAIR3*) gene appears to be involved in the regulation microtubule assembly and disassembly. In *fra2/erh3* mutants trichomes are underbranched; also, other cell types show morphogenesis defects (Burk et al., 2001; Webb et al., 2002). *FRA2/ERH3* encodes for a katanin-p60 protein, suggesting that it functions as a microtubule-severing protein (Burk et al., 2001; Webb et al., 2002). In *fs* (*fass*)/*ton2* (*toneau2*) mutants, shape changes of various cell types have been correlated with severe distortions of the microtubule cytoskeleton (Traas et al., 1995; McClinton and Sung, 1997). Therefore, it is likely that the unbranched trichome phenotype in *fs* mutants (Torres-Ruiz and Jürgens, 1994) is also linked to the microtubule phenotype. *TON2* encodes a novel protein phosphatase 2A regulatory subunit, suggesting that microtubule organization in plants is controlled by the phosphorylation and dephosphorylation of proteins (Camilleri et al., 2002). Mutations in the *SPIKE1* gene results in underbranched trichomes along with morphogenesis defects in various cell types. Microtubule organization is misregulated in *spk1* mutants and the recent cloning of *SPK1* revealed that it encodes an adapter protein involved in the integration of extracellular signals with the cytoskeletal organization (Qiu et al., 2002). These observations are supported by drug inhibitor studies that revealed distinct roles of actin and tubulin during trichome cell morphogenesis (Mathur et al., 1999; Szymanski et al., 1999; Mathur and Chua, 2000). Although the inhibition of the actin cytoskeleton causes irregularities in the directionality of cell expansion, drugs disturbing the microtubule cytoskeleton result in reduced trichome branching.

To further elucidate the molecular mechanisms underlying branch formation, we have studied the *STI* (*STICHEL*) gene. *sti* mutants exhibit the strongest branch phenotype: All trichomes are unbranched. Positional cloning revealed that *STI* encodes a novel protein containing a domain with sequence similarity to eubacterial DNA-polymerase III γ -subunits. However, endoreduplication levels were unaltered in *sti* mutants and in plants overexpressing *STI*. Also, the

general organization of the actin and microtubule cytoskeleton in *sti* mutants was not affected. Our analysis of various *sti* alleles and transgenic lines overexpressing *STI* suggests that *STI* is a regulator of branch number rather than a requirement for branching.

RESULTS

Map-Based Cloning of the *STICHEL* Gene

We isolated the *STI* gene by molecular mapping of recombination breakpoints in about 1,800 F_1 events from a *sti* (*Landsberg erecta* [Ler]) \times wild-type (Columbia-0 [Col]) cross and chromosomal walking. The *STI* gene was initially mapped north of the two molecular markers (m497 and m246) on chromosome II and further fine mapped to an interval of about 2 cM between ve012 and m246 as shown in Figure 1. This interval is spanned by two overlapping yeast (*Saccharomyces cerevisiae*) artificial chromosomes (YACs), CIC11A4 and CIC9D8. The right end of CIC9D8 and the molecular marker ve012 were used to establish a chromosomal walk with bacterial artificial chromosomes (BACs). Five additional CAPS markers were identified in this region that enabled us to map the *STI* gene to a 50-kb interval on the BAC F8N6 that lies within a region sequenced by the TIGR group of the Arabidopsis Genome Initiative (BACs T8K22 and T16F16). The annotation of the genomic sequence of this interval revealed seven potential genes (for details, see Fig. 1).

To identify *STI*, we tested several candidate genes for allele-specific polymorphisms by sequencing genomic DNA of *Ler* wild type and two *sti* alleles. Both *sti* alleles have mutations in a gene containing a domain with sequence similarity to the eubacterial DNA-polymerase III γ -subunits (GenBank no. At2g02480). We confirmed that this gene represents the *STI* gene by identifying mutations in the genomic sequence of an additional five *sti* alleles. To determine the genomic structure of the *STI* gene, we used reverse transcription (RT)-PCR to amplify cDNA fragments from total RNA of young rosettes. Sequencing of the amplified cDNA fragments revealed a 3.6-kb open reading frame and the comparison with the genomic sequence showed that the *STI* gene contains six exons. The 3' end of the cDNA was determined by RACE-PCR. The transcription start could not be determined by RACE. However, we could amplify a cDNA fragment containing 120 bp upstream of the predicted START codon. This region contains one or more STOP codons in all possible frames, indicating that the predicted START codon initiating an open reading frame of 1,218 codons is correct. Figure 2 shows the *STI* cDNA sequence and the predicted *STI* protein sequence. The mutations found in *sti* alleles include small deletions and single-nucleotide exchanges that are predicted to result in premature STOP codons as well as mutations that are

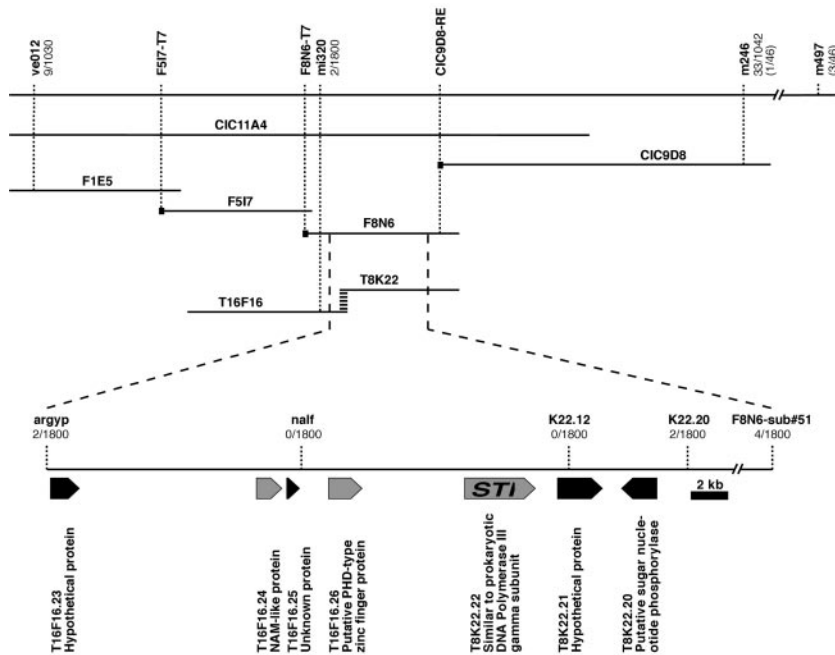


Figure 1. Mapping of the *STI* gene. The genetic map between ve012 and m497 at the northern part of chromosome II is shown at the top. Below, Relative orientation of relevant YAC and BAC clones is displayed. BACs of the Institut für Genbiologische Forschung (IGF) library (F1E5, F517, and F8N6) were identified and mapped using probes marked as black squares. BACs of the TAMU library (T8K22 and T16F16, GenBank accession nos. AC004136 and AC005312, respectively) are from the mi320-nga1145 contig sequenced by The Institute for Genomic Research (TIGR; <http://www.tigr.org/tdb/e2k1/ath1/>) and were mapped based on sequence comparison with sequenced fragments of the IGF BACs. Molecular markers used for mapping are shown together with the recombination frequencies. The blowup of the chromosomal region between the two markers *argyp* and F8N6-sub#51 shows a higher resolution map and the predicted genes in the *argyp*-K22.12 interval, including the gene identification and name. Genes shaded in gray were sequenced for two or more *sti* alleles and the corresponding wild-type *Ler*.

predicted to impair the correct splicing (for details, see Fig. 2). All changes are likely to eliminate the activity of mutant STI proteins. A sequence comparison between the two ecotypes (*Ler* and *Col*) revealed a number of nucleotide changes, 10 of which are predicted to cause amino acid changes (for details, see Fig. 2). In addition, we found a number of deletions and insertions ranging from 5 to 11 bp in some of the introns (data not shown), most of which are not predicted to affect splicing. Differential splicing was observed in intron 5. Some of the subcloned RT-PCR-amplified *Ler*-cDNA fragments were missing nine nucleotides at the beginning of the sixth exon, resulting from the utilization of an alternative splicing acceptor site (for details, see Fig. 2). As judged from the relative signal intensities when directly sequencing RT-PCR products, the two splicing events occur approximately with the same frequency (data not shown).

Putative Functional Domains of the STI Gene Product

The *STI* gene encodes a protein of 1,218 amino acid residues with a predicted molecular mass of 135.3 kD. Sequence comparison with other known proteins and motifs identified three putative functional domains. A large domain between amino acids 454 and 799 shows sequence similarity to eubacterial DNA-polymerase III γ -subunits (Fig. 3A). The prokaryotic DNAPol III γ -subunit is the main component of the γ -complex, which is important for the formation of the replication initiation complex with the dimeric β -subunit. In principle, the DNA polymerase III is able to perform DNA replication without the β -subunit, but the processivity is lower by several

orders of magnitude. Upon ATP binding, the γ -complex loads the β -subunit onto a primer DNA template. Dissociation of the γ -complex from the β -subunit to allow the polymerase to bind the β -subunit requires ATP hydrolysis (Bertram et al., 1998). The similarity is 49% to 55% (identity 29%–35%) within the homology region. Similarity to the family of 36- to 40-kD ATP-binding subunits of replication factor C (RFC, also known as activator 1), the archaeobacterial and eukaryotic functional counterparts of the bacterial γ subunit (Chen et al., 1992a, 1992b), is less pronounced (42%–44% similarity, 23%–27% identity). Figure 3B shows the alignment of STI with this group of proteins, including the putative RFC from *Arabidopsis*. The latter is that member of a class of four putative RFCs in *Arabidopsis* that shows highest sequence similarity with the eukaryotic RFCs (Fig. 5). Figure 4 illustrates that STI and four STI homologs from *Arabidopsis* represent a phylogenetically separate branch, thereby defining a new, potentially plant-specific, subfamily among the γ -subunit homologs. The five proteins of this subfamily are markedly larger than the relatively small RFC proteins and the prokaryotic DNAPol III γ subunits and show sequence similarity outside the RFC/ γ subunit domain (Fig. 5).

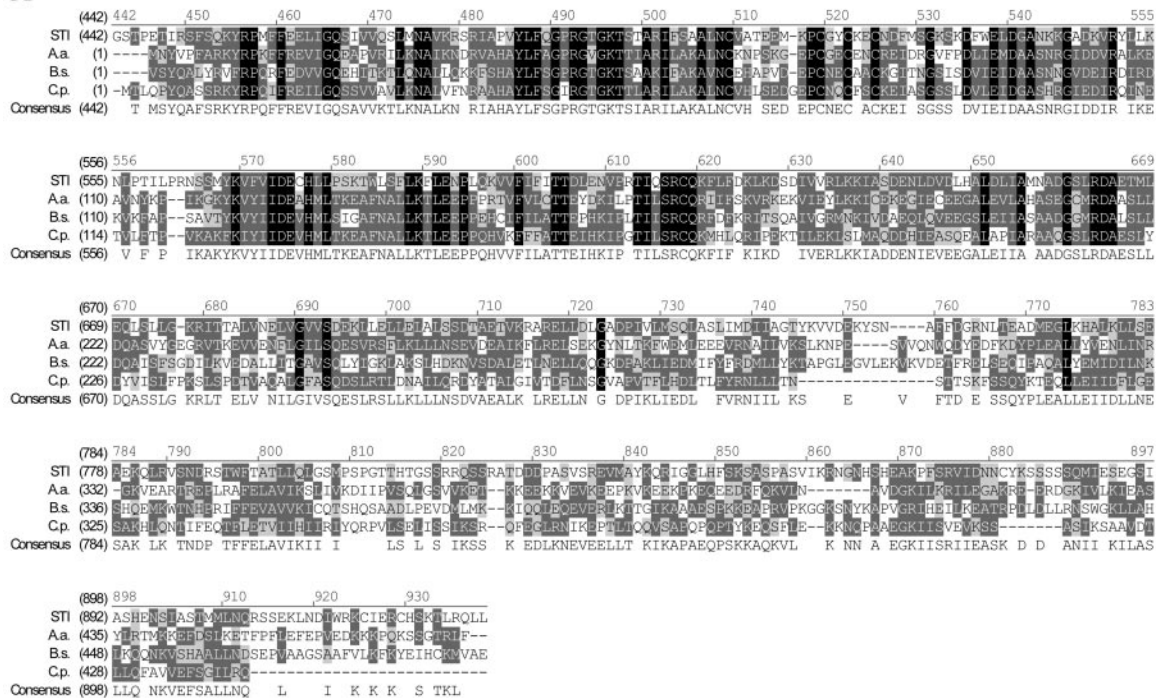
Two regions, one between amino acids 273 and 304 and a second between amino acids 425 and 449, show similarity to PEST domains known to mediate rapid protein degradation. According to the score calculated based on the PEST hypothesis by Rodgers et al. (1986), the two PEST domains found in STI have a very high score of 9.24 and 9.58.

Three nuclear localization signals (NLSs) suggest that STI is targeted to the nucleus with a probability

frame with the normal reading frame and provided with an acceptable Kozak sequence (Kozak, 1984). The weak *sti-40* allele has a G to A exchange five nucleotides downstream from the splice donor site of the second intron, which presumably impairs normal splicing. The *sti-XT1* allele has a one-nucleotide deletion that results in a frame shift at position 2,596, leading to a STOP three codons downstream. *sti-56* has a G to A exchange at the splice acceptor site of the third intron, resulting in a frame shift and a STOP codon at position 2882. *sti-EMU* shows a one-nucleotide deletion resulting in a frame shift at position 3,070, leading to the altered amino acid sequence M L K L V A A W K A D E Q S R C K G STOP. The following amino acids are altered in Col: 145 (V to M), 277 (I to T), 355 (S to N), 439 (G to E), 826 (S to A), 828 (I to V), 889 (A to G), 891 (V to I), 1,023 (K to T), and 1,177 (H to Q). Conserved functional domains are underlined: presumptive PEST boxes (dotted), presumptive bipartite nuclear localization sequences (double underlines), and the DNA polymerase III γ -subunit homology domain (single underline).

Figure 2. *Ler* cDNA and predicted protein sequence of STI. STOP codons preceding the translation START are marked in bold italics. Intron positions are marked with >< above the nucleotide sequence. Intron 5 is differentially spliced in *Ler*, leading to the deletion of 5 K Q at the positions 1,182 through 1,184 (marked in bold italics) in approximately one-half of the transcripts. Other *Ler*/Col-specific polymorphisms and mutations in various *sti* alleles (with their name in parentheses) are indicated above the nucleotide sequence (lowercase letters for nucleotide exchanges, Δ for deletions). Premature STOP codons resulting from mutations are marked in bold. *sti-47*, although a weak allele, has a point mutation resulting in the earliest observed STOP mutation at position 109. Possibly, an alternative START codon (position 484, marked in bold italics) is used that is in

A



B

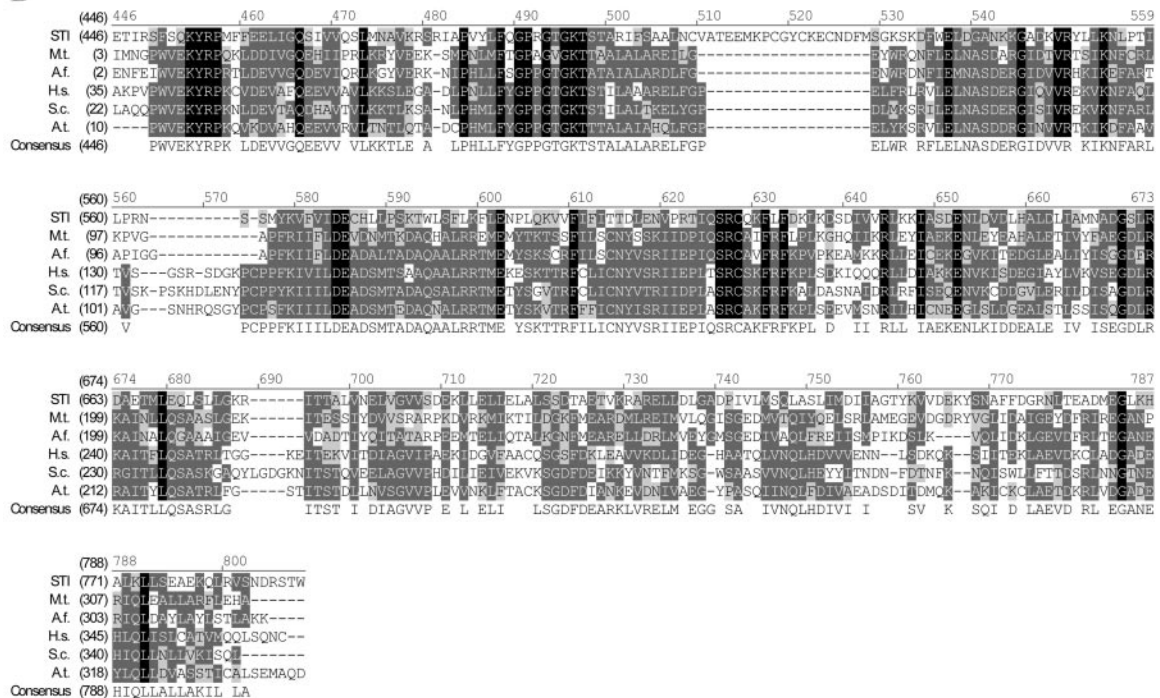


Figure 3. Sequence alignment of STI with prokaryotic DNA polymerase III γ -subunits and the small subunits of eukaryotic and archaeobacterial replication factor Cs. A, Alignment of the *STICHEL* sequence with related protein sequences of prokaryotic DNA polymerase III γ -subunits. Black-shaded amino acids are identical, dark gray-shaded amino acids are conserved, and light gray indicates weak similarity. The numbering at the top corresponds to amino acid positions in STI. A.a., *Aquifex aeolius* (aq 1855); B.s., *Bacillus subtilis* (Bsu0019); C.p., *Chlamydia pneumoniae* (CPn0040). B, Alignment of STI with related protein sequences of the small subunit of replication factor C. A.t., *Arabidopsis* (At1g2169); A.f., *Archaeoglobus fulgidus* (AF20608); M.t., *Methanobacterium thermoautotrophicum* (MTH241); S.c., yeast (YSCRFC2); H.s., human (*Homo sapiens*).

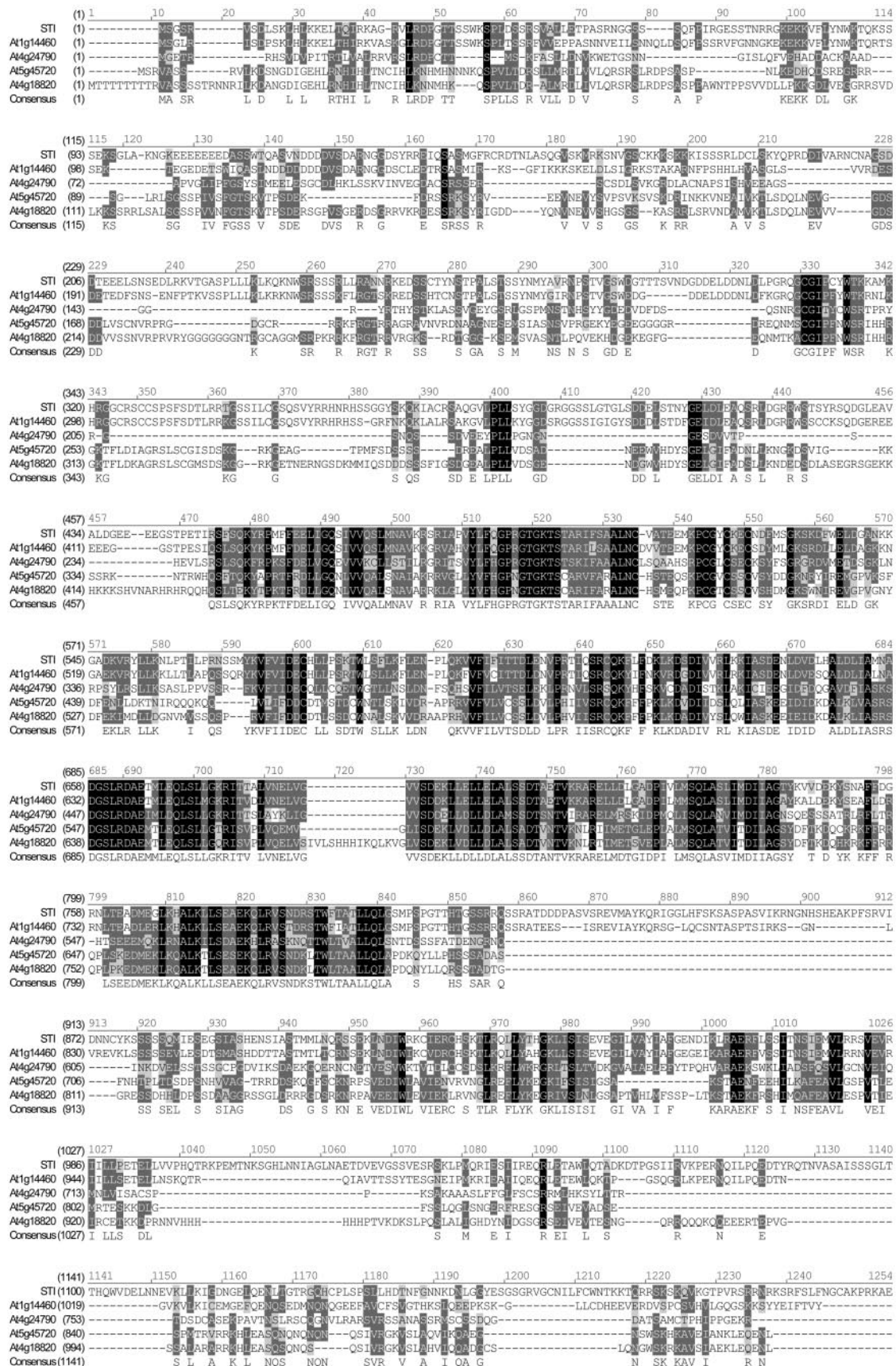


Figure 4. (Legend appears on facing page.)

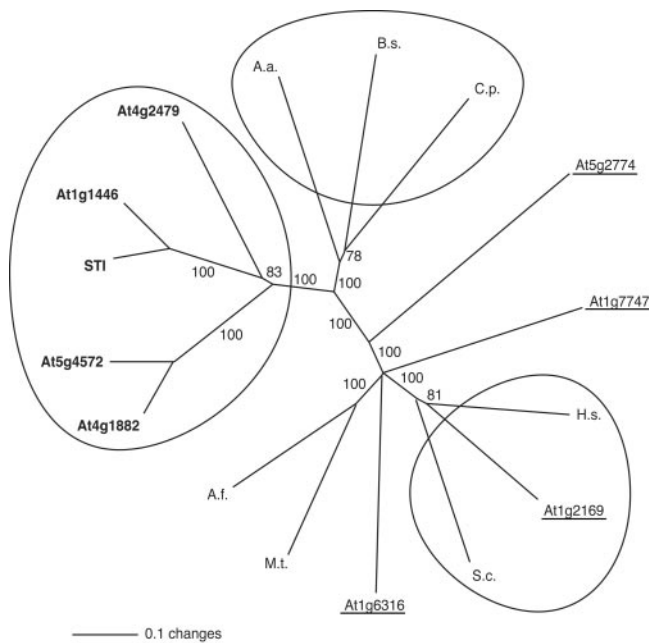


Figure 5. Phylogenetic tree of the STI, the DNA polymerase III γ -subunit, and the RFC small subunit family. The phylogenetic tree of STI, the DNA polymerase III γ subunit and the RFC small subunit family were calculated using only the core homology region corresponding to amino acids 449 to 799 in STI. The phylogenetic distance is shown as an unrooted dendrogram. The scale bar indicates 10% changes of amino acids. The bootstrap values are indicated for each branch. The five closest related STI homologs are bold and the four putative RFC-like proteins in Arabidopsis are underlined. The five closest STI homologs fall in a class that is separate from both, the prokaryotic DNA polymerase III γ -subunits and the eukaryotic RFC small subunits (the three groups are marked by circles). Note that only one of the Arabidopsis RFCs, At1g2169, is in the same group as the known eukaryotic RFC small subunits. A.a. = *A. aeolius* (aq 1855); B.s., *B. subtilis* (Bsu0019); C.p., *C. pneumoniae* (CPn0040); A.f., *A. fulgidus* (AF20608); M.t., *M. thermoautotrophicum* (MTH241); S.c., yeast (YSCRFC2); H.s., human.

not with *try* (Folkers et al., 1997). Although *nok* and *try* mutant trichomes display a similar branch phenotype, the formation of up to five branch points, the two genes act in two different pathways. In *try* mutant trichomes, endoreduplication is increased 2-fold and, as a consequence, trichome cells are bigger and form more branches. In *nok* mutants, the production of extra branches is not coupled to the number of endoreduplication cycles. Our analysis of double and triple mutants with the weak *sti-40* allele revealed that, in contrast to *sti-EMU*, the increase in the DNA content can rescue branching in the *sti-40* background (Table II; Fig. 6). Although *sti-40* trichomes have one branch point with a frequency of 78%, the double mutant with *nok* or *try* has mainly two branch points and the triple mutant *sti-40 nok try* has up to four branch points

(Table II; Fig. 6). In the corresponding double mutant combinations with the stronger *sti-EMU* allele, a similar trend is observed (Folkers et al., 1997), though the rescue effect by *nok* is not enhanced by *try* (data not shown). It is important to also note that one of the strongest *sti* alleles, the x-ray-induced *sti-XT1*, is partially rescued in a *nok* mutant background (Fig. 6G). To test whether a reduction in the DNA content reduces trichome branching in the weak *sti-40* mutant, *sti-40 gl3* and *sti-40 gl3 nok* mutant combinations were generated. The decrease in endoreduplication in the *gl3* background eliminates branching almost completely, and this effect can be rescued by additionally removing *NOK* in the triple mutant (Table II; Fig. 6I).

The analysis of *sti*-alleles and their function in various mutant backgrounds suggest that *STI* acts in a dosage-dependent manner. To test this further, we transformed 35S:*STI* into *sti*-mutants. Sixty-seven transgenic lines were studied for the rescue of the mutant phenotype. Seventeen lines showed a weak rescue, and 34 showed complete rescue with up to three branches. In addition, we found in 11 lines trichomes with more than two branch points, occasionally up to five branch points (Fig. 6, J and K). Semiquantitative RT-PCR analysis of the 35S:*STI*-specific expression levels did not reveal clear differences in the RNA levels between lines exhibiting weaker or stronger rescue (Table III; Fig. 7A). Thus, in summary, the overexpression of *STI* does not only rescue the *sti* phenotype, but also leads to extra branch formation.

Also, in 35S:*STI* lines, stem trichomes that are normally unbranched exhibited up to two branch points (Fig. 6L), suggesting that organ-specific differences in trichome branching are controlled by *STI*.

STI Is Expressed in All Organs

To test where *STI* is expressed, we performed a northern-blot analysis. *STI* expression was found at about the same levels in all organs tested: rosette leaves, siliques, stem, and roots (Fig. 7B). This finding was confirmed by RT-PCR using primer pairs that specifically amplify *STI* but not its homologs (data not shown). Also, rosette leaves from *gl1* (*glabra1*) mutants that are devoid of trichomes show *STI* expression at approximately the same levels as wild type. These data show that *STI* is expressed ubiquitously in all organs rather than in a trichome-specific manner.

STI Is Not Involved in the Regulation of Endoreduplication

As judged by the visual inspection of 4',6-diaminophenylindole-stained whole mounts, *sti* trichomes

Figure 4. Sequence comparison between STI with its closest homologs. STI is a member of a class of five homologs that share sequence similarity outside the DNA polymerase III γ -subunit/RFC domain. Black-shaded amino acids are identical, dark gray-shaded amino acids are conserved, and light gray indicates weak similarity.

Table I. Allelic series of the *sti* mutation

Alleles	No. of Branch Points ^a				No. of Trichomes ^b
	0	1	2	3	
Wild type (<i>Ler</i>)	–	3	97	–	622
Wild type (<i>Col</i>)	–	–	92	8	925
40 (<i>Ler</i>)	22	78	–	–	593
47 (<i>Ler</i>)	55	45	–	–	458
Cs430 (<i>Col</i>)	96	4	–	–	999
EMU (<i>Ler</i>)	97	3	–	–	486
56 (<i>Ler</i>)	99	1	–	–	512
EM1 (<i>Ler</i>)	100	–	–	–	107
XT1 (<i>Ler</i>)	100	–	–	–	101

^a Percentage of trichomes. ^b Trichomes were counted on the third and fourth leaves of seven or more plants.

appear to have a DNA content similar to wild type. To exclude that reduced branching in *sti* mutants is due to a reduction in the DNA content, we measured the DNA content in trichomes of the weak *sti-40* allele and the strong *sti-XT1* allele. In both alleles, it was on average 37.5 ± 18 C ($n = 50$) and 41.4 ± 15 C ($n = 58$), respectively, which closely corresponds to wild-type measurements (38 ± 17 C, $n = 49$). Also, *sti try* double mutants showed the expected 2-fold increase in the DNA content (*sti-40 try*, 93 ± 35 C, $n = 51$; *sti-XT1 try*, 84 ± 33 C, $n = 57$; and *try*, 80 ± 37 C, $n = 49$), again indicating that DNA replication in *sti* trichomes is not impaired.

Conversely, overbranched trichomes in *35S:STI* plants did not have an increased DNA content. This was studied in two independent lines. In both lines, trichomes had a DNA content indistinguishable from wild type (38 ± 15 C, $n = 149$; 37 ± 16 C, $n = 60$).

STI Does Not Affect the Actin or Microtubule Organization

In trichomes, actin and tubulin appear to have distinct roles such that during the early growth phase until branching is completed, microtubules play a major role, whereas actin is important during cell expansion (Mathur et al., 1999; Szymanski et al., 1999; Mathur and Chua, 2000). To study whether the actin or the microtubule cytoskeleton are affected in *sti* mutants, we compared their arrangement in wild type and *sti* mutants.

To monitor the actin cytoskeleton, we used a transgenic *35S::GFP-talin* line. This line ubiquitously expresses the green fluorescent protein (GFP) fused to the C terminus of mouse talin, which binds to F actin and, thus, decorates the actin in vivo (Rees et al., 1990; McCann and Craig, 1997; Kost et al., 1998). In mature wild-type trichomes, the cortex of the cell is characterized by a fine actin network. The more prominent bundles in the center of the cell are mainly oriented with respect to the longitudinal axis. In *sti* mutants, the actin distribution was indistinguishable from wild type, indicating that STI is not involved in the regulation of the actin cytoskeleton (data not shown).

To visualize the microtubule distribution in living trichomes, we used a transgenic *35S::GFP-MAP4* line that expresses GFP fused to the microtubule-associated protein 4 (Mathur and Chua, 2000). In mature wild-type trichomes, the microtubules are found mainly at the cell cortex where microtubule filaments are initially radially and later, after branch formation is completed, longitudinally oriented (Fig. 8). Also, *sti* mutants showed a shift from an initial radial microtubule organization to a longitudinal orientation.

DISCUSSION

Although the genetic and cell biological analysis of trichome branching provides a well-defined framework for the formal logic of the system, little is

Table II. Branching phenotype in multiple mutants

Alleles	No. of Branch Points ^a					No. of Trichomes ^b
	0	1	2	3	4	
<i>sti-40</i>	22	78	–	–	–	593
<i>sti-40 nok-122</i>	–	10	90	–	–	185
<i>sti-40 gl3</i>	100	–	–	–	–	291
<i>sti-40 gl3l+</i>	68	32	–	–	–	115
<i>sti-40 gl3 nok-122</i>	–	72	28	–	–	242
<i>try-EM1 sti-40</i>	–	81	19	–	–	169
<i>try-EM1 sti-40 nok-122</i>	–	–	47	41	12	176

^a Percentage of trichomes. ^b Trichomes were counted on the third and fourth leaves of seven or more plants.

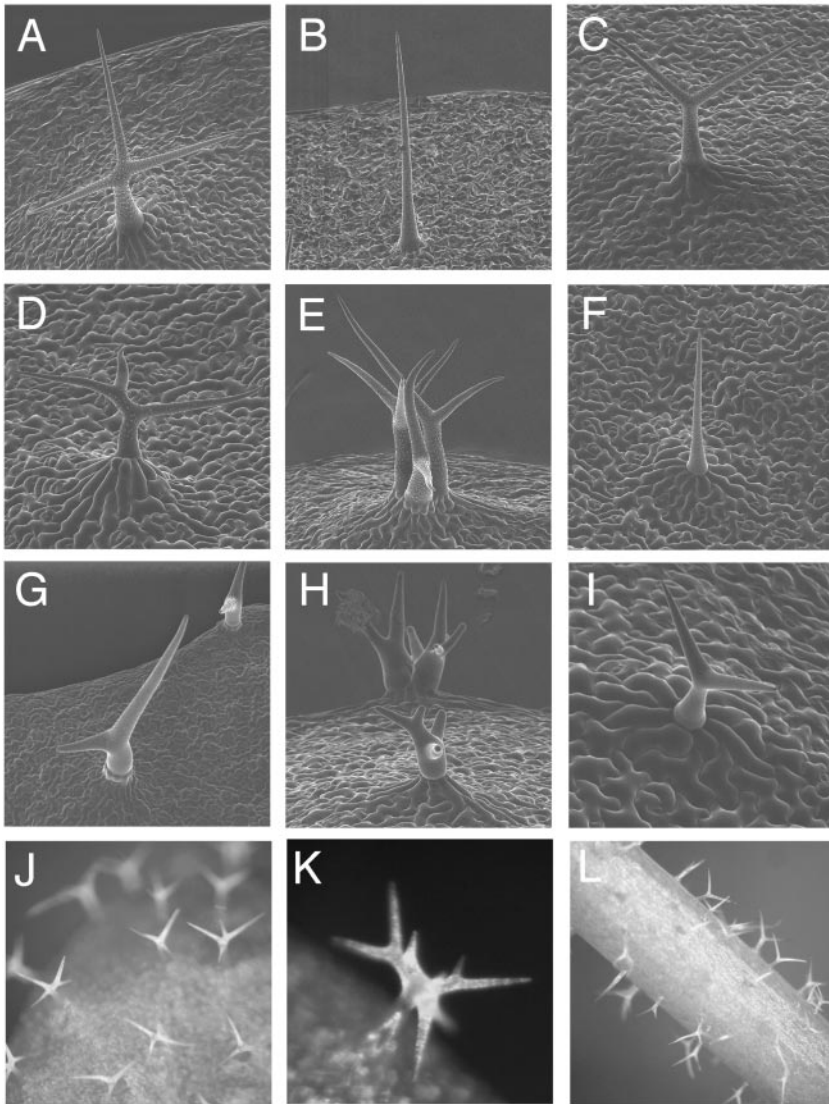


Figure 6. Single and double mutant phenotypes of combinations with different *sti* alleles. Scanning electron micrographs of trichomes. A, wild type; B, *sti-EMU*; C, *sti-40*; D, double mutant *sti-40 nok-122*; E, double mutant *try-EM1 sti-40*; F, double mutant *sti-40 gl3*; G, double mutant *sti-XT1 nok-122*; H, triple mutant *try-EM1 sti-40 nok-122*; I, triple mutant *sti-40 nok-122 gl3*; J, 35S:*STI* rosette leaf with four branched trichomes; K, 35S:*STI* leaf trichome with seven branch points; L, 35S:*STI* stem trichomes with branches.

known about the underlying molecular mechanisms. The molecular analysis of several branching mutants revealed links to the control of the microtubule function at different regulation levels, including the microtubule-based transport processes (Oppenheimer et al., 1997), the regulation of microtubule assembly and disassembly (Burk et al., 2001; Webb et al., 2002), and the control of microtubule organiza-

tion (Traas et al., 1995; Camilleri et al., 2002; Folkers et al., 2002; Kim et al., 2002; Qiu et al., 2002). Although these findings provide an excellent entry point into the understanding of the final steps of cell morphogenesis, earlier steps such as the control of branch initiation and its spatial control remain misunderstood. Because genetic analysis has suggested that *STI* plays a key role in these early processes we

Table III. Branching phenotype in multiple overexpressors

Lines	No. of Branch Points ^a					No. of Trichomes ^b
	0	1	2	3	4	
No. 12	2	58	40	—	—	422
No.67	1	38	61	—	—	370
No. 60	—	4	92	4	—	379
No.8	—	1	61	38	—	360
No.7	—	—	58	42	—	219

^a Percentage of trichomes.

^b Trichomes were counted on the third and fourth leaves of seven or more plants.

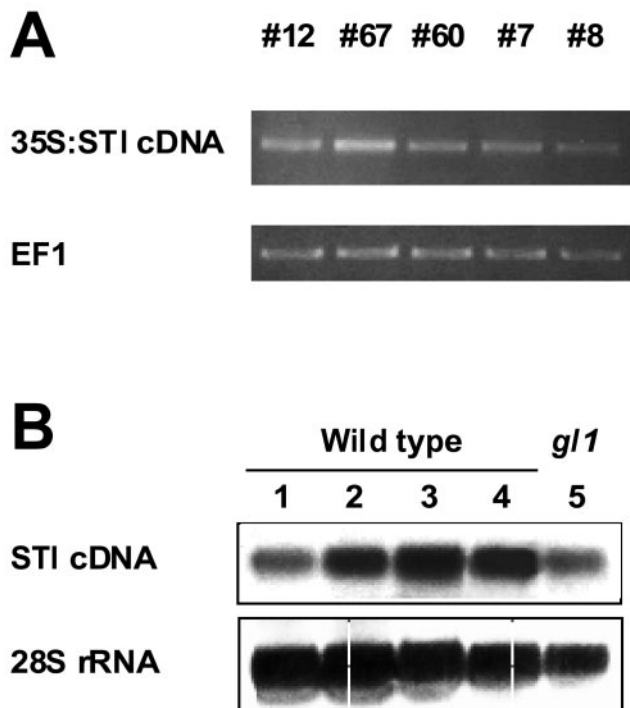


Figure 7. STI expression. A, Analysis of expression levels in 35S:STI lines by semiquantitative RT-PCR. The numbers of the lines correspond to those in Table III. The elongation factor1 EF1 was used as a control. B, Northern-blot analysis of *STI* expression in different plant organs: lane 1, roots; lane 2, stems; lane 3, siliques; and lanes 4 and 5, rosette leaves. 28S rRNA served as load control for the blot.

have isolated the *STI* gene by a positional cloning approach. The molecular characterization of seven *sti* alleles revealed allele-specific polymorphisms that are all predicted to severely impair either splicing and/or protein function. Therefore, we conclude that we have cloned the *STI* gene.

The Role of STI in Cell Morphogenesis

Three lines of evidence suggest that *STI* regulates branching in a dosage-dependent manner. First, mutations in the *STI* gene do not simply eliminate its function, but depending on the severity of the defect, intermediate phenotypic defects are also observed. This suggests that less *STI* activity results in fewer branches. Second, conversely, lines overexpressing *STI* can trigger extra branch formation. A third line of evidence supporting a regulatory role of *STI* in branch formation comes from the genetic analysis of double mutants. In a previous study, the finding that *sti* mutants can be rescued in double mutants with *nok* but not with *try* has led to the assumption that *STI* and *NOK* might specifically counteract each other (Folkers et al., 1997). However, our findings that weak *sti* alleles can also be rescued by *try* and that the additional removal of *TRY* in a *sti nok* background results in an even better rescue suggests that mutations in the *sti* gene can be bypassed in several

ways. This suggests that *STI* is not required to make branches, but involved in the regulation of their number.

The cell biological analysis of *sti* mutants revealed no deviation from wild type at the subcellular level. One criterion to monitor cell differentiation is the timing and extent of cell vacuolization. Reduced vacuolization was found to be associated with severe growth abnormalities of root hairs in *rhd3* mutants (Galway et al., 1997). Vacuolization in *sti* mutant trichomes, however, was normal (data not shown). A second important aspect is the organization and function of the actin and microtubule cytoskeleton. The general organization of both cytoskeletal elements was normal, suggesting that *STI* is not involved in the control of the microtubule or actin organization.

Potential Molecular Function of STI

The sequence similarities of *STI* to other proteins provides few clues about its molecular function. The presence of NLS domains and a DNA-polymerase III γ -subunit/RFC domain suggest that *STI* might be involved in the regulation of DNA replication. This, however, seems to be unlikely because the ploidy level in trichomes is normal in *sti* mutants and in lines overexpressing *STI*, indicating that replication is not affected in both situations. Consistent with this interpretation is the finding that *STI* belongs to a group of five genes that is clearly distinct from the putative Arabidopsis RFC genes. These five genes also show sequence similarity outside the DNA-polymerase III γ -subunit/RFC domain, suggesting that they may have adopted a new plant-specific role. If *STI*, as suggested by the NLS motives, is localized to the nucleus, *STI* might be involved in the regulation of gene expression. However, because it lacks any similarity to known transcription factors, this would be by a novel mechanism. An attractive alternative would be that *STI* is involved directly in the formation of branches in the cytoplasm. In analogy to the role of DNA-polymerase III γ -subunit/RFC, *STI* could mediate the formation of protein complexes initiating branch formation. Localization studies should allow the first insights in these questions.

MATERIALS AND METHODS

Plant Material and Genetic Analysis

Plants were grown at constant illumination at 23°C. Wild-type strains used in this work were *Ler* and *Col*. Single mutant lines were isolated from the F_2 progeny of plants mutagenized with ethyl methanesulfonate as described (Mayer et al., 1991) with the exception of the *sti* allele *sti-Cs430*, which was isolated from a T-DNA insertion mutagenesis screen by Csaba Koncz (Max-Planck-Institut, Cologne, Germany). Double mutants were created by preselecting F_2 plants displaying the phenotype of one of the parents and selecting F_3 plants for a new phenotype. Double mutants were backcrossed with the parental lines to verify their genotype. Triple mutants were created from double mutants that shared one of the mutant backgrounds following the

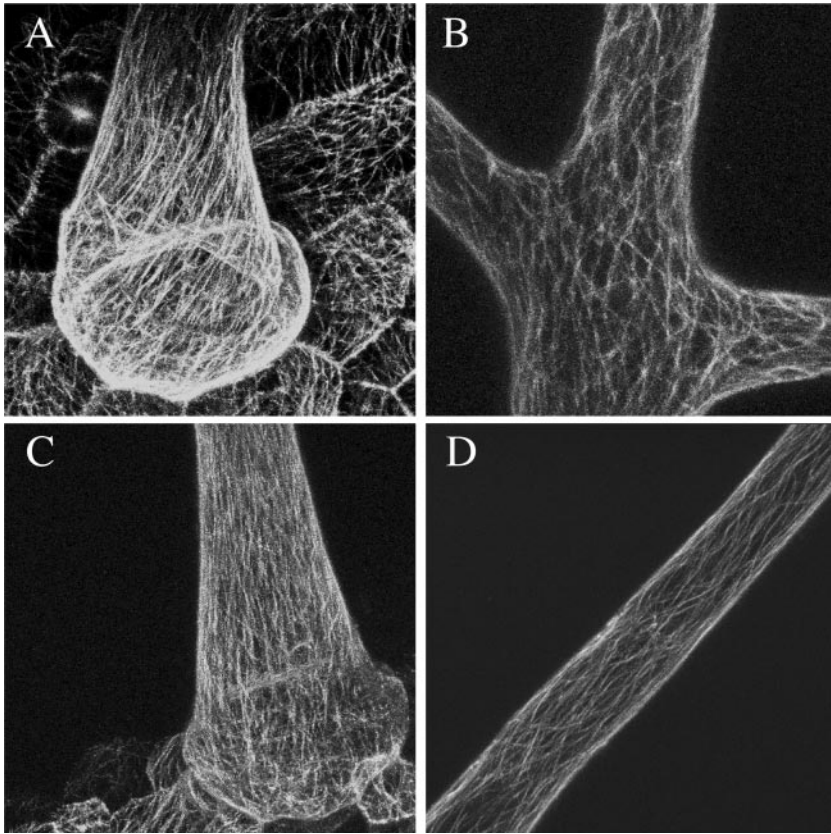


Figure 8. Microtubule organization in wild-type and *sti* mutant trichomes. A, Microtubule organization at the base of a wild-type trichome. B, Microtubule organization at the branch point of a wild-type trichome. C, Microtubule organization at the base of a *sti* trichome. D, Microtubule organization in the mid-region of an *sti* mutant trichome.

same procedure. The following single and double mutants have been described previously: *sti-EMU*, *sti-EM1*, *sti-XT1*, *try-EM1*, and *try-EM1 sti-EMU* (Hülkamp et al., 1994); *sti-40*, *nok-122*, *nok-122 sti-EMU*, and *nok-122 sti-40* (Folkers et al., 1997); and *gl3* (Koornneef et al., 1982).

Molecular Cloning of the *STI* Gene

Plant genomic DNA was prepared as described previously (Leutwiler et al., 1984; Lukowitz et al., 1996). For initial mapping, the RFLP marker probes m246 and m497 modified by Fabri and Schöffner were used (Fabri and Schöffner, 1994). m246 was further used as a CAPS marker (Konieczny and Ausubel, 1993). The YAC contig was established by Zachgo et al. (1996; <http://weeds.mgh.harvard.edu/goodman/>). The hybridization probes for the chromosome walk were generated by modified thermal asymmetric interlaced-PCR (Liu and Whittier, 1995) with the nested primers 5'-CAG CAA CCG CAC CTG TGG C-3', 5'-GAT GCG TCC GGC GTA GAG-3', and 5'-GAG TCG AAC GCC CGA TC-3' for the right end of CIC9D8 and 5'-GAT TAA GTT GGG TAA CGC CAG GG-3', 5'-AGT CAC GAC GTT GTA AAA CGA CG-3', and 5'-GTA ATA CGA CTC ACT ATA GGG C-3' for the BAC T₇ ends. The BAC clones from the library IGF-BAC 122 (Mozo et al., 1998) were received from Katharina Henschel (Resource Center/Primary Database of the German Human Genome Project, Berlin).

New CAPS marker were generated by the following strategy: BACs were shotgun subcloned into pBluescript SK⁺ (Stratagene, La Jolla, CA). Inserts of appropriate size were sequenced and primers for genomic amplification were designed with the McVector 4.5 software (Kodak Scientific Imaging Systems, New Haven, CT). PCR products were tested for ecotype-dependent restriction enzyme polymorphisms. To convert the RFLP marker mi320 (Robert Whittier, Mitsui Plant Biotechnology, Tsukuba, Japan) into a CAPS marker, the 1.3-kb RFLP marker probe (received from the Arabidopsis Biological Resource Center, Columbus, OH, stock no. CD3-281) was used to identify a 6.4-kb *Hind*III fragment from BAC F2012. An ecotype-specific polymorphism was identified as described above. Sequence information on ve012 was provided by David Bouchez (Laboratoire de Biologie Cellulaire, Institut National de la Recherche Agronomique, Versailles, France). K22.12,

K22.20, *argyp*, and *nalf* were designed based on sequence information submitted by the TIGR group of the Arabidopsis Genome Project (see Fig. 1). The CAPS marker primers were: ve012, 5'-CCC ACC ATT GAA GGA GAA AAC AG-3' and 5'-CAG CAG AGA AGA AGT AAA CCG CC-3' (*Eco*130I); mi320, 5'-CTG TCT TTT GGT ATT TCG GG-3' and 5'-GAA CGA TCA ATG TGT TGG AAG-3' (*Hind*III); *argyp*, 5'-GTT GCT CGG CAG AAG TTA G-3' and 5'-AGG TAC TCG CAC AGT ACG C-3' (*Csp*6I); *nalf*, 5'-GCT GAA ATA TCA TTG TGC C-3' and 5'-GCC CAT TAA AGG ATA GTG G-3' (length polymorphism); K22.12, 5'-CTA TAG CAA ACT CAT GGC-3' and 5'-AGT CTA AGA TGA TGG TGG-3' (*Mva*I); K22.20, 5'-CAT GAA ATT CCC TTC CAC-3' and 5'-ATC GTT ACC AAA GCA TCC-3' (*Ava*I); and F8N6-sub#51, 5'-AGT CTC CCT TAG TTT GAG TG-3' and 5'-CTG GAA TAG AAG CAT TAC C-3' (*Hpa*II). Further details are available on request.

Primers for amplification and sequencing of gene candidates were also created based on the sequence information provided by TIGR. Sequencing was carried out on an ABI Prism (Perkin-Elmer Applied Biosystems, Foster City, CA) sequencing equipment according to the manufacturer's instructions. The *STI*-transcribed sequence was amplified using the 5'-TGA AAA CGC GAA GCT GAG AGA G-3' and 5'-CGA ACA GGA GTT CCC TTG-3' primer pair from cDNA obtained by oligo(dT)-primed RT of RNA isolated from rosettes with four to five leaves. The 3' end was obtained using the oligo(dT) primer and the gene-specific nested primers 5'-CTG ATA AAG ACA CAC CTG GAT CG-3' and 5'-ATC GCC AAA CTA ACG TAG C-3'. 5'-RACE PCR was performed with the 5'-RACE System for Rapid Amplification of cDNA Ends, version 2.0 (Life Technologies/Gibco-BRL, Cleveland) according to the manufacturer's instructions using the specific nested primers 5'-CAT TAA CAC TAG CTT GCG TCC AC-3' and 5'-CTC TTC TTC CTT ACC ATT CTT AG-3'. It yielded no products related to the *STI* gene. The sequence of the 5' region, including 120 bp of upstream untranslated sequence, was obtained using the 5'-TTG CAC AGG TTT TGA AAT GTC AG-3' and 5'-CTC TTC TTC CTT ACC ATT CTT AG-3' primer pair.

The expression levels of *STI*-overexpressing plants were estimated by semiquantitative RT-PCR analysis. RNA was isolated using Dynabeads (Dynal Biotech, Oslo) and treated with DNaseI to remove genomic DNA. RT

PCR was carried out with Titan One tube RT-PCR mix (Roche Diagnostics, Indianapolis). The primer pair SNT-70-forward (5'-CGA CGG TAT CGA TAA GCT TG-3') and SNT-70-reverse (5'-ACA CCT AAA ACC ACC GAA G-3') were designed to only amplify the 35S:STI transcript. No transcript was detected in wild-type plants after 35 cycles.

Sequence Analysis

Proteins related to STICHEL were identified by BLAST search (Altschul et al., 1990). Sequence alignment was performed with the Multiple Sequence Alignment Program (Huang, 1994) at the Baylor College of Medicine Search Launcher (<http://searchlauncher.bcm.tmc.edu/multi-align/>), BOXSHADE version 3.21 by K. Hoffmann and M. Baron at EmbNet (<ftp.isrec.isb-sib.ch>), and Vector NTI alignX-Block version 7.0. Functional domains were identified by searching the protein sequence against the Pfam database (Bateman et al., 1999) and PSORT 6.4 (<http://psort.nibb.ac.jp>). The phylogenetic tree was created using distance, parsimony, and maximum likelihood criteria using the PAUP 4.0B.1 program (Swofford, 1998). The confidence of branching was determined using 1,000 bootstrap resamplings.

Cytological Methods and Pictures

Confocal laser-scanning microscopy was done with the TCS-NT program (Leica Microsystems, Bensheim, Germany). 4',6-Diamino-phenylindole staining and nDNA content measurements were performed as described previously (Hülkamp et al., 1994). For scanning electron micrographs freshly cut leaves were mounted without fixing and immediately analyzed at 10 kV. Pictures were processed with the Aldus Freehand 7.0 (Aldus Corp., Seattle) and Adobe Photoshop 3.0 (Adobe Systems Inc., Mountain View, CA) software.

ACKNOWLEDGMENTS

We thank members of the authors' lab for critically reading the manuscript. We thank Birger Marin for excellent help with dendrogram calculations.

Received September 10, 2002; returned for revision October 25, 2002; accepted November 14, 2002.

LITERATURE CITED

- Aeschbacher R, Schiefelbein JW, Benfey PN (1994) The genetic and molecular basis of root development. *Annu Rev Plant Physiol Plant Mol Biol* **45**: 25–45
- Altschul SF, Gish W, Miller W, Myers EW, Lipman DJ (1990) Basic local alignment search tool. *J Mol Biol* **215**: 403–410
- Bateman A, Birney E, Durbin R, Eddy SR, Finn RD, Sonnhammer EL (1999) Pfam 3.1: 1313 multiple alignments match the majority of proteins. *Nucleic Acids Res* **27**: 260–262
- Bertram JG, Bloom LB, Turner J, O'Donnell M, Beechem JM, Goodman MF (1998) Pre-steady state analysis of the assembly of wild type and mutant circular clamps of *Escherichia coli* DNA polymerase III onto DNA. *J Biol Chem* **273**: 24564–24574
- Burk DH, Liu B, Zhong R, Morrison WH, Ye ZH (2001) A katanin-like protein regulates normal cell wall biosynthesis and cell elongation. *Plant Cell* **13**: 807–827
- Camilleri C, Azimzadeh J, Pastuglia M, Bellini C, Grandjean O, Bouchez D (2002) The *Arabidopsis* TONNEAU2 gene encodes a putative novel protein phosphatase 2A regulatory subunit essential for the control of the cortical cytoskeleton. *Plant Cell* **14**: 833–845
- Chen M, Pan Z-Q, Hurwitz J (1992a) Sequence and expression in *Escherichia coli* of the 40-kDa subunit of activator 1 (replication factor C) of HeLa cells. *Proc Natl Acad Sci USA* **89**: 2516–2520
- Chen M, Pan Z-Q, Hurwitz J (1992b) Studies of the cloned 37-kDa subunit of activator 1 (replication factor C) of HeLa cells. *Proc Natl Acad Sci USA* **89**: 5211–5215
- Fabrizi CO, Schäffner AR (1994) An *Arabidopsis thaliana* RFLP mapping set to localize mutations to chromosomal regions. *Plant J* **5**: 149–156
- Folkers U, Berger J, Hülkamp M (1997) Cell morphogenesis of trichomes in *Arabidopsis*: differential control of primary and secondary branching by branch initiation regulators and cell growth. *Development* **124**: 3779–3786
- Folkers U, Kirik V, Schobinger U, Falk S, Krishnakumar S, Pollock MA, Oppenheimer DG, Day I, Reddy AR, Jurgens G et al. (2002) The cell morphogenesis gene *ANGUSTIFOLIA* encodes a CtBP/BARS-like protein and is involved in the control of the microtubule cytoskeleton. *EMBO J* **21**: 1280–1288
- Galway ME, Heckman J, Schiefelbein JW (1997) Growth and ultrastructure of *Arabidopsis* root hairs: the *rhd3* mutation alters vacuole enlargement and tip growth. *Planta* **201**: 209–218
- Huang X (1994) On global sequence alignment. *Comput Appl Biosci* **10**: 227–235
- Hülkamp M, Folkers U, Grini P (1998) Cell morphogenesis in *Arabidopsis*. *BioEssays* **20**: 20–29
- Hülkamp M, Folkers U, Schnittger A (1999) Trichome development in *Arabidopsis thaliana*. *Int Rev Cytol* **186**: 147–178
- Hülkamp M, Misera S, Jurgens G (1994) Genetic dissection of trichome cell development in *Arabidopsis*. *Cell* **76**: 555–566
- Kim GT, Shoda K, Tsuge T, Cho K-H, Uchimiya H, Yokoyama R, Nishitani K, Tsukaya H (2002) The *ANGUSTIFOLIA* gene of *Arabidopsis*, a plant CtBP gene, regulates leaf-cell expansion, the arrangement of cortical microtubules in leaf cells and expression of a gene involved in cell-wall formation. *EMBO J* **26**: 1267–1279
- Kirik V, Bouyer D, Schobinger U, Bechtold N, Herzog M, Bonneville JM, Hülkamp M (2001) CPR5 is involved in cell proliferation and cell death control and encodes a novel transmembrane protein. *Curr Biol* **11**: 1891–1895
- Konieczny A, Ausubel FM (1993) A procedure for mapping *Arabidopsis* mutations using co-dominant ecotype-specific PCR-based markers. *Plant J* **4**: 403–410
- Koornneef M, Dellaert LWM, Veen JHVd (1982) EMS- and radiation-induced mutation frequencies at individual loci in *Arabidopsis thaliana*. *Mut Res* **93**: 109–123
- Kost B, Mathur J, Chua N-H (1999) Cytoskeleton in plant development. *Curr Opin Plant Biol* **2**: 462–470
- Kost B, Spielhofer P, Chua NH (1998) A GFP-mouse talin fusion protein labels plant actin filaments in vivo and visualizes the actin cytoskeleton in growing pollen tubes. *Plant J* **16**: 393–401
- Kozak M (1984) Compilation and analysis of sequences upstream from the translational start site in eukaryotic mRNAs. *Nucleic Acids Res* **12**: 857–872
- Leutwiler LS, Hough-Evans BR, Meyerowitz EM (1984) The DNA of *Arabidopsis thaliana*. *Mol Gen Genet* **194**: 15–23
- Liu Y-G, Whittier RF (1995) Efficient isolation and mapping of *Arabidopsis thaliana* T-DNA insert junctions by thermal asymmetric interlaced PCR. *Plant J* **8**: 457–463
- Lukowitz W, Mayer U, Jurgens G (1996) Cytokinesis in the *Arabidopsis* embryo involves the syntaxin-related KNOLLE gene product. *Cell* **84**: 61–71
- Luo D, Oppenheimer DG (1999) Genetic control of trichome branch number in *Arabidopsis*: the roles of the *FURCA* loci. *Development* **126**: 5547–5557
- Marks MD (1997) Molecular genetic analysis of trichome development in *Arabidopsis*. *Annu Rev Plant Physiol Plant Mol Biol* **48**: 137–163
- Mathur J, Chua NH (2000) Microtubule stabilization leads to growth reorientation in *Arabidopsis thaliana* trichomes. *Plant Cell* **12**: 465–477
- Mathur J, Spielhofer P, Kost B, Chua N-H (1999) The actin cytoskeleton is required to elaborate and maintain spatial patterning during trichome cell morphogenesis in *Arabidopsis thaliana*. *Development* **126**: 5559–5568
- Mayer U, Ruiz RAT, Berleth T, Misera S, Jurgens G (1991) Mutations affecting body organization in the *Arabidopsis* embryo. *Nature* **353**: 402–407
- McCann RO, Craig SW (1997) The I/LWEQ module: a conserved sequence that signifies F-actin binding in functionally diverse proteins from yeast to mammals. *Proc Natl Acad Sci USA* **94**: 5679–5684
- McClinton RS, Sung ZR (1997) Organization of cortical microtubules at the plasma membrane in *Arabidopsis*. *Planta* **201**: 252–260
- Mozo T, Fischer S, Shizuya H, Altmann T (1998) Construction and characterization of the IGF *Arabidopsis* BAC library. *Mol Gen Genet* **258**: 562–570

- Oppenheimer D** (1998) Genetics of plant cell shape. *Curr Opin Plant Biol* **1**: 520–524
- Oppenheimer DG, Pollock MA, Vacik J, Szymanski DB, Ericson B, Feldmann K, Marks MD** (1997) Essential role of a kinesin-like protein in *Arabidopsis* trichome morphogenesis. *Proc Natl Acad Sci USA* **94**: 6261–6266
- Pepper A, Delaney T, Washburn T, Poole D, Chory J** (1994) DET1, a negative regulator of light-mediated development and gene expression in *Arabidopsis*, encodes a novel nuclear-localized protein. *Cell* **78**: 109–116
- Perazza D, Herzog M, Hülskamp M, Brown S, Dorne A, Bonneville J** (1999) Trichome cell growth in *Arabidopsis thaliana* can be depressed by mutations in at least five genes. *Genetics* **152**: 461–476
- Qiu JL, Jilk R, Marks MD, Szymanski DB** (2002) The *Arabidopsis* SPIKE1 gene is required for normal cell shape control and tissue development. *Plant Cell* **14**: 101–118
- Rees DJ, Ades SE, Singer SJ, Hynes RO** (1990) Sequence and domain structure of talin. *Nature* **347**: 685–689
- Rodgers S, Wells R, Rechsteiner M** (1986) Amino acid sequences common to rapidly degraded proteins: the PEST hypothesis. *Science* **234**: 364–368
- Swofford DL** (1998) PAUP, Phylogenetic Analysis Using Parsimony (and Other Methods). Version 4. Sinauer Associates, Sunderland, MA
- Szymanski DB, Marks MD, Wick SM** (1999) Organized F-actin is essential for normal trichome morphogenesis in *Arabidopsis*. *Plant Cell* **11**: 2331–2348
- Torres-Ruiz RA, Jürgens G** (1994) Mutations in the FASS gene uncouple pattern formation and morphogenesis in *Arabidopsis* development. *Development* **120**: 2967–2978
- Traas J, Bellini C, Nacry P, Kronenberger J, Bouchez D, Caboche M** (1995) Normal differentiation patterns in plants lacking microtubular preprophase bands. *Nature* **375**: 676–677
- Webb M, Jouannic S, Foreman J, Linstead P, Dolan L** (2002) Cell specification in the *Arabidopsis* root epidermis requires the activity of ECTOPIC ROOT HAIR 3—a katanin-p60 protein. *Development* **129**: 123–131
- Wilhelmi LK, Preuss D** (1999) The mating game: pollination and fertilization in flowering plants. *Curr Opin Plant Biol* **2**: 18–22
- Zachgo EA, Wang ML, Dewdney J, Bouchez D, Camilleri C, Belmonte S, Huang L, Dolan M, Goodman HM** (1996) A physical map of chromosome 2 of *Arabidopsis thaliana*. *Genome Res* **6**: 19–25